Obtaining Concentration Profiles from Computer Simulation Structure Factors

Andrew J. Schultz,[‡] Carol K. Hall,*[,†] and Jan Genzer[†]

Department of Chemical and Biomolecular Engineering, North Carolina State University, Raleigh, North Carolina 27695, and Department of Chemical and Biological Engineering, University at Buffalo, The State University of New York, Buffalo, New York 14260

Received December 11, 2006
Revised Manuscript Received February 7, 2007

The structure factor, $S(\mathbf{q})$, is an important analysis tool for analyzing the structure of macromolecular crystals,[1,2] block copolymers,[3] micelles,[4] and the glass transition.[5] As the Fourier transform of the density profile, $S(\mathbf{q})$ gives a quantitative description of the concentration fluctuations in a system as a function of the fluctuation frequency and direction. $S(\mathbf{q})$ can be obtained experimentally from scattering experiments or can be extracted from simulation data on particle positions. In the past, $S(\mathbf{q})$ has been used to determine the size and morphology of micelles, the degree of ordering, the identity of an ordered structure, and even the interaction strength between components of a copolymer.[6−8]

The concentration profile of any structure can be estimated by finding the inverse Fourier transform of $S(\mathbf{q})$. However, to do this, it is often necessary to assume that the structure conforms to a model and then, by comparing the model $S(\mathbf{q})$ to the measured structure factor, determine the actual morphology or characteristic size of the structure. However, this approach is not unambiguous in that many different concentration profiles could have the same $S(\mathbf{q})$ because the phase angle cannot be obtained from experiment.

In this Communication, we describe a new method for extracting concentration profiles from molecular simulation data based on direct analysis of $S(\mathbf{q})$, thus avoiding the aforementioned ambiguity associated with assuming a model geometry.[9,10] The method can also be extended to calculate the average concentration profile from multiple simulation snapshots. We also show that it is possible to identify which parts of $S(\mathbf{q})$ are related to which geometrical features of the structure. Finally, we show how to compensate for capillary waves' broadening effect on the average concentration profile.

We first review the mathematical relationship between the simulation particle positions and $S(\mathbf{q})$ and the relationship between $S(\mathbf{q})$ and the concentration profile. $S(\mathbf{q})$ for component A can be calculated using

$$S(\mathbf{q}) = \frac{(\sum_j \cos(\mathbf{q}\cdot\mathbf{r}_j))^2 + (\sum_j \sin(\mathbf{q}\cdot\mathbf{r}_j))^2}{N} \tag{1}$$

where $\mathbf{q}$ is the wave vector, $\mathbf{r}_j$ is the location of particle j, and N is the number of particles in the system. The set of possible wave vectors $\mathbf{q}$ is limited by the periodic boundaries which restricts $\mathbf{q}$ to an integer number of wavelengths within the simulation box.

The concentration profile can be written as a sum of multiple sine waves:

$$\rho_A(\mathbf{r}) = \rho_A(1 + \sum_k \beta_{Ak} \sin(\mathbf{q}_k\cdot\mathbf{r} + \theta_{Ak})) \tag{2}$$

where $\rho_A(\mathbf{r})$ is the number density of component A at location $\mathbf{r}$, ρ_A is the average density of component A in the system, and β_{Ak} is the amplitude and θ_{Ak} is the phase angle. Since $S(\mathbf{q})$ is the Fourier transform of the concentration profile, we can determine the sine wave parameters, β and θ, from

$$\beta_{Ak} = \frac{2}{N_A}\sqrt{S_A(\mathbf{q}_k)\,N} \tag{3}$$

$$\theta_{Ak} = \tan^{-1}\left(\frac{\sum_j \cos(\mathbf{q}_k\cdot\mathbf{r}_j)}{\sum_j \sin(\mathbf{q}_k\cdot\mathbf{r}_j)}\right) \tag{4}$$

This allows us to obtain β_{Ak} and θ_{Ak} from quantities that we calculate in the simulation and reconstruct the concentration profile for component A as the sum of multiple sine waves using eq 2. When reconstructing the concentration profile, it is necessary to choose a wave vector cutoff, $|\mathbf{q}_{cut}|$ in order to smear out the effect of each individual particle.

To illustrate the process of determining the concentration profile from a single simulation snapshot, consider calculating the concentration profile of a system of microphase-separated diblock copolymers from simulation data.[11] We performed a simulation of 1600 polymer molecules, each modeled as a freely rotating chain of 20 tangent square-well spheres at a packing fraction of 0.35, a volume fraction of A monomers, f_A of 0.3, and a reduced temperature chosen such that $\chi N = 48.4$. Under these conditions, the copolymers form a hexagonal array of eight cylinders pointing in the x direction. In Figure 1a, we plot $S(q)/N_b$ vs $|\mathbf{q}|\sigma$, where N_b is the total number of beads in the system. The primary peak is visible at $|\mathbf{q}^*|\sigma = 0.52$; the secondary peak at $\sqrt{7}|\mathbf{q}^*|\sigma = 1.38$ is also prominent.

The interface of the cylindrical structure is shown in Figure 1b as an isosurface at $\rho_A(\boldsymbol{r})/\rho = 0.5$, with $\rho_A(\boldsymbol{r})$ calculated using eq 2 from the single snapshot structure factor in Figure 1a; ρ is the average number density for all components in the system. When calculating the concentration profile, we chose a wave vector cutoff of $|q_{cut}|\sigma = 2$ and also excluded fluctuations whose structure factor was below $S_{cut}/N_b = 10^{-5}$ for computational convenience and because these fluctuations make a negligible contribution to the concentration profile. The interface is noticeably "bumpy" even though χN is well above the order−disorder transition ($\chi N = 33$ for this volume fraction[11]).

The average concentration profile of an ordered structure can be obtained by calculating the concentration profiles of many snapshots and then averaging them together. It is not correct to simply calculate the average structure factor for a number of snapshots and then apply eq 2 because the phase angles and structure factor magnitudes vary from snapshot to snapshot. Instead, it is necessary to use eq 2 to calculate the concentration profile for each snapshot and average these together. However, before averaging the concentration profiles, we need to translate the individual concentration profiles to a common position. This can be done by determining the translation that minimizes

* To whom correspondence should be addressed. E-mail: hall@turbo.che.ncsu.edu.
[†] North Carolina State University.
[‡] University at Buffalo, The State University of New York.

10.1021/ma062836d CCC: $37.00
Published on Web 03/15/2007

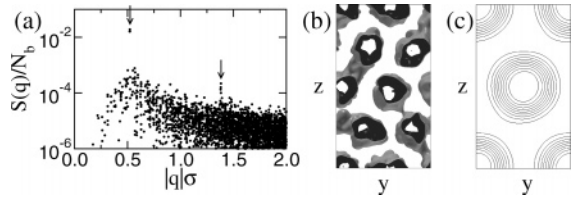

Figure 1. (a) Structure factor from a single snapshot of hexagonally spaced cylinders with ordered peaks indicated by arrows, (b) isosurface corresponding to (a), and (c) contour plot of the average concentration profile, with each contour representing a change of 0.1 in the volume fraction of component A.

differences in the phase angles associated with primary peaks between different snapshots.

As an example, we apply this method to obtain the average concentration profile for the cylinder-forming block copolymer system we described previously. The average concentration profile calculated from the 100 snapshots taken over a simulation of length $t^* \equiv (t/\sigma)(k_BT/m)^{1/2} = 2000$ reduced time units is displayed in Figure 1c as a contour plot, with each contour corresponding to a change of 0.1 in the volume fraction ($\rho_A(r)/\rho$) of component A. As previously, we have used a wave vector cutoff of $|\mathbf{q}_{cut}|\sigma = 2$ and a structure factor cutoff of $S_{cut} = 10^{-5}N_b$. The cylinders appear as concentric circles at the center and at each corner of the figure. The inner and outer circles correspond to a $\rho_A(r)/\rho$ equal to 1.0 and 0.0, respectively. The average concentration profile as a contour plot is easier to interpret since it does not include the bumps associated with noise in the single snapshot.

Next, we demonstrate how the current method can be used to determine how a given portion of the structure factor data contributes to the concentration profile. In our simulations, the block copolymer with $f_A = 0.35$ self-assembles into lamellar sheets at high values of χN. But when χN is near the disorder transition, the lamellar sheets develop perforations. These perforations are not arranged hexagonally,[12−16] but are disordered instead.[17,18] Disordered perforations are difficult to account for in mean-field theories, which are designed to account for either order or randomness, but not partial order. Likewise, it is difficult to identify disorder in scattering experiments because such experiments are sensitive only to the ordered parts of the structure. Hajduk et al. detected a metastable phase between the gyroid and lamellae phases using rheological methods and concluded that it was a lamellae with disordered perforations based on the similarity of its structure factor and the structure factor of lamellae.[17] Imai et al. investigated nonionic surfactants and found a diffuse peak at wavelengths less than the primary peak position and argued that it was due to disordered perforations.[18] In simulations, "detecting" the perforations is trivial, but this is not particularly helpful to others attempting to identify phases in block copolymer experiments. However, by relating the perforations to specific features in the structure factor, we can identify which parts of the structure factor signal the existence of a perforated lamellar structure.

We performed a simulation of a block copolymer system at $f = 0.35$ and $\chi N = 43.0$, which resulted in perforated lamellar structures oriented perpendicular to the y axis. The structure factor of component A resulting from a single snapshot is shown in Figure 2a. For details of the simulations, see ref 11. The structure factor peaks at $\mathbf{q}^*$, $2\mathbf{q}^*$, $3\mathbf{q}^*$, and $4\mathbf{q}^*$ indicate lamellar ordering. Calculating the concentration profile from the single-snapshot structure factor, again using a wave vector cutoff of $2/\sigma$ and a minimum structure factor cutoff of 10^{-5}, yields the concentration profile whose isosurface at $\rho_A(\boldsymbol{r})/\rho = 0.5$ is shown

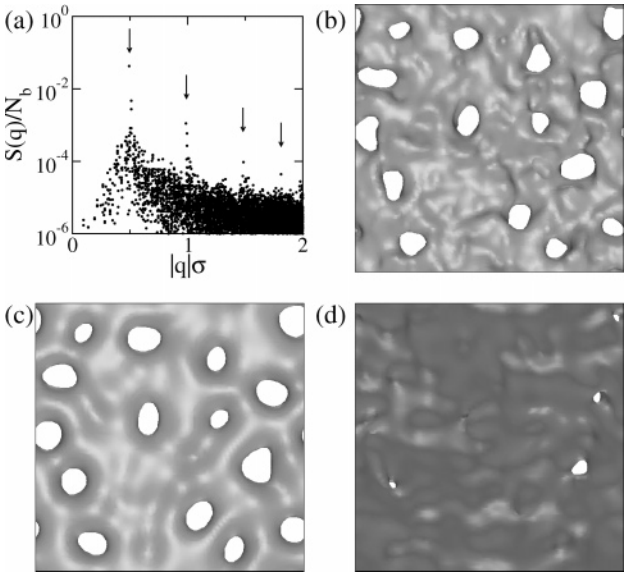

Figure 2. (a) Structure factor for a single snapshot of perforated lamellae. Isosurfaces of perforated lamellar sheet using (b) $|\mathbf{q}|\sigma < 2$, (c) $0.3 < |\mathbf{q}|\sigma < 0.7$, but excluding those with $|q_y| = |\mathbf{q}^*|$ (except for the primary peak itself), and (d) the primary peak and all wave vectors excluded from (c).

in Figure 2b. The perforations are distributed throughout the layer, with little or no ordering between them. Since the perforations are disordered, there are no ordered peaks in the structure factor to signal their existence. Instead, the perforations must correspond to some other part of the structure factor.

In order to determine which parts of the structure factor contribute to the lamellar perforations, we reconstructed the concentration profile with various parts of the structure factor included or excluded. We found that the minimal set of wave vectors needed to reconstruct a concentration profile with disordered perforations is the primary peak, $|\mathbf{q}^*|$, and $0.3 < |\mathbf{q}|\sigma < 0.7$, but excluding wave vectors with $|q_y| = |\mathbf{q}^*|$. The isosurface resulting from that set of wave vectors is shown in Figure 2c. We also constructed concentration profiles using the primary peak and all the wave vectors that were not included in constructing Figure 2c. The resulting isosurface, shown in Figure 2d, contains only a few very small perforations. On the basis of the existence of perforations in Figure 2c and the relative lack of perforations in Figure 2d, we conclude that the primary peak, $|\mathbf{q}^*|$ and wave vectors with $0.3 < |\mathbf{q}|\sigma < 0.7$ but excluding $|q_y| = |\mathbf{q}^*|$ are responsible for the lamellar perforations at $\chi N = 43.0$. This result contrasts with the conclusion of Imai et al.,[18] who found that the in-plane fluctuations ($|q_y| = 0$) in their experiments correspond to lamellar perforations. Although in-plane fluctuations contribute to the perforations in our simulations, they are not as important as those with $0 < |q_y| < |\mathbf{q}^*|$.

Another potential application of our method is to remove the effect of capillary waves from the average concentration profile. Because capillary waves shift various parts of the structure perpendicular to the lamellar interface, the concentration profile flattens and the interface between the domains broadens. This artificial broadening increases with system size and hampers the interpretation of the concentration profiles. Although the broadening of an interface by capillary waves has been considered before,[19−21] we can use the structure factor to treat the capillary waves more directly.

As an example of a system affected by capillary waves, we consider a system containing symmetric ($f = 0.5$) block copolymers with strong interactions ($\chi N = 96.8$), which forms lamellae. We simulated a single lamellar sheet in a simulation

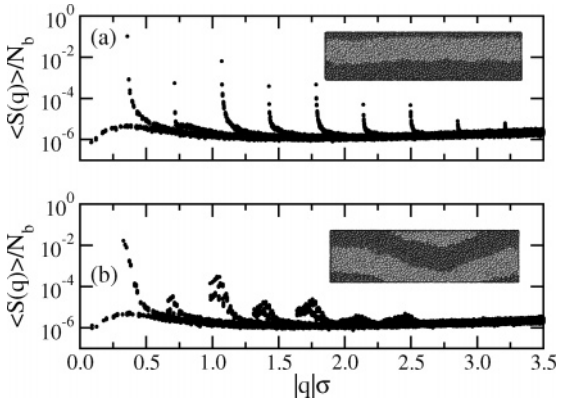

Figure 3. Simulation structure factors of (a) unperturbed lamellae without capillary waves and (b) perturbed lamellae with capillary waves. Simulation snapshots are shown for each system.

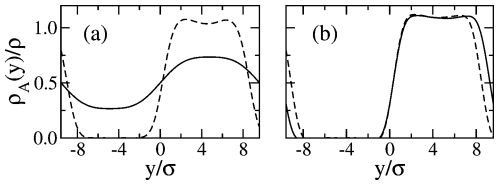

Figure 4. Average concentration profiles corresponding to (a) the unperturbed system without capillary waves (dashed) and the perturbed system with capillary waves (solid) and (b) the same systems after applying capillary wave removal.

box with dimensions $73.7\sigma \times 17.6\sigma \times 73.7\sigma$. The average $S(\mathbf{q})$ for this "unperturbed" system, shown in Figure 3a with a simulation snapshot, has a primary peak at $|\mathbf{q}^*|\sigma = 0.357$ and $\langle S\rangle/N_b = 0.104$ and 8 distinct secondary peaks. We adjusted the simulation box lengths to $70.7\sigma \times 19.2\sigma \times 70.7\sigma$ and reequilibrated the system, with the expectation that the larger box length in the y dimension would induce a buckling effect[22] characteristic of capillary waves. The $S(\mathbf{q})$ of the "perturbed" system is shown in Figure 3b along with a simulation snapshot; the $S(\mathbf{q})$ for the perturbed system is qualitatively different from that for the unperturbed system. The primary peak is much weaker than that in Figure 3a, and there are only six secondary peaks. Although the $S(\mathbf{q})$ peaks in Figure 3b are less intense than those in Figure 3a, the primary peak "tail" (the curve running from the peak maximum to the noise level) is more pronounced. The secondary peak "tails" also have strong intensity, exceeding the intensities of the secondary peaks themselves.

The average concentration profiles constructed without capillary removal for component A in the perturbed and unperturbed systems are shown in Figure 4a. The concentration profile for the unperturbed system has a sharp interface between domain A and B, with the reduced concentration, $\rho_A(\mathbf{r})/\rho$, of component A exceeding 1 within domain A near the interface and reaching 0 within domain B. The concentration profile for the perturbed system has a much broader interface. Although the concentration profiles for the perturbed system are "correct", they are a poor representation of the system's state because they do not reflect the actual compositions of the domains, or the sharpness of the interface between them, which are similar to those in the unperturbed system. The dramatic difference between the concentration profiles in the perturbed and unperturbed case is also inconsistent with the difference in thermodynamic properties of the two systems: the potential energy of the perturbed system is only 1.7% less than the unperturbed system, and the average polymer radius of gyration is only 1.7% greater.

Since the concentration profiles perpendicular to the lamellar interface, $\rho_A(y)/\rho$ vs y at any particular value of x and z, are relatively unaffected by the capillary waves, the average concentration profile can be obtained by averaging over the various x and z. The following procedure is used. We calculate local values (at each x and z) for the structure factor intensities and phase angles. Then, we translate the local concentration profiles such that the local phase angles of the primary wave vectors have a common value. Finally, we determine the structure factor and phase angles of this new structure, i.e., the structure in which the local concentration profiles are all aligned, and calculate the average concentration profile.

We applied the capillary removal technique to both the perturbed and unperturbed block copolymer systems. Unlike our previous calculations, we do not apply any cutoff to the intensity of $S(\mathbf{q})$ because constructive interference from many weak capillary waves can result in a noticeable difference in the concentration profile, even when the individual contributions are nearly negligible. We also use a larger wave vector cutoff, $|\mathbf{q}_{cut}|\sigma = 3.5$, because of the existence of high-frequency fluctuations with high intensity in the unperturbed system. In both systems, we calculated local concentration profiles at 100 x and z points, sampled randomly to ensure that the method is not artificially sensitive to the structure's lateral periodicity. The resulting average concentration profiles, shown in Figure 4b, at the AB interface ($y/\sigma = 0$) are nearly identical for both the perturbed and unperturbed cases. The similarity of these profiles is much more consistent with the similar thermodynamic properties of the two systems and confirms that we are accurately representing the average local concentration profile.

While the concept of using $S(\mathbf{q})$ to determine geometric structure is well established and used in crystallography, its application in simulation is unique because the phase angles are known, making it possible to make a direct determination of the geometry. Although concentration profiles can be obtained from other methods, such as particle position histogramming, use of $S(\mathbf{q})$ can provide greater insight into the structure's geometry. We hope that having the ability to more precisely relate $S(\mathbf{q})$ to geometric features will allow simulators to help in the interpretation of experiments when neither geometry nor phase angles are available.

While we have focused on block copolymers in this Communication, the techniques could be applied to other systems such as photonic crystals and periodic nanocomposites and colloids. The structure factor could also be used to construct and analyze concentration profiles for macrophase-separated or micellar systems with well-defined structure, even in the absence of periodicity. Beyond concentration profiles, the techniques could be applied to any property, such as kinetic temperature or molecular orientation, that is desired as a continuous spatial profile, but can only be measured at discrete points.

Acknowledgment. This work was supported by the GAANN Computational Sciences Fellowship of the U.S. Department of Education and the Office of Energy Research, Basic Sciences, Chemical Science Division of the U.S. Department of Energy under Contract DE-FG05-91ER14181.

References and Notes

(1) Wilson, A. J. C. *Nature (London)* **1992**, *355*, 472.
(2) Brünger, A. T. *Nature (London)* **1992**, *355*, 472.
(3) Bates, F. S.; Fredrickson, G. H. *Annu. Rev. Phys. Chem.* **1990**, *41*, 525.
(4) Castelletto, V.; Hamley, I. W. *Curr. Opin. Colloid Interface Sci.* **2002**, *7*, 167.
(5) Tölle, A. *Rep. Prog. Phys.* **2001**, *64*, 1473.

(6) Fulton, J. L.; Pfund, D. M.; McClain, J. B.; Romack, T. J.; Maury, E. E.; Combes, J. R.; Samulski, E. T.; Desimone, J. M.; Capel, M. *Langmuir* **1995**, *11*, 4241.
(7) Floudas, G.; Ulrich, R.; Wiesner, U. *J. Chem. Phys.* **1999**, *110*, 652.
(8) Bates, F. S. *Macromolecules* **1985**, *18*, 525.
(9) Schultz, A. J. Modeling and Computer Simulation of Block Copolymer/Nanoparticle Composites. Ph.D. Thesis, North Carolina State University, Dept. of Chem. Eng., 2004.
(10) Martinez-Veracoechea, F. J.; Escobedo, F. A. *Macromolecules* **2005**, *38*, 8522.
(11) Schultz, A. J.; Hall, C. K.; Genzer, J. *J. Chem. Phys.* **2002**, *117*, 10329.
(12) Khandpur, A. K.; Förster, S.; Bates, F. S.; Hamley, I. W.; Ryan, A. J.; Bras, W.; Almdal, K.; Mortensen, K. *Macromolecules* **1995**, *28*, 8796.
(13) Matsen, M. W.; Bates, F. S. *Macromolecules* **1996**, *29*, 1091.
(14) Laradji, M.; Shi, A.-C.; Noolandi, J.; Desai, R. C. *Macromolecules* **1997**, *30*, 3242.
(15) Ahn, J.-H.; Zin, W.-C. *Macromolecules* **2000**, *33*, 641.
(16) Zhu, L.; Huang, P.; Cheng, S. Z. D.; Ge, Q.; Quirk, R. P.; Thomas, E. L.; Lotz, B.; Wittmann, J.-C.; Hsiao, B. S.; Yeh, F.; Liu, L. *Phys. Rev. Lett.* **2001**, *86*, 6030.
(17) Hajduk, D. A.; Takenouchi, H.; Hillmyer, M. A.; Bates, F. S.; Almdal, K. *Macromolecules* **1997**, *30*, 3788.
(18) Imai, M.; Kawaguchi, A.; Saeki, A.; Nakaya, K.; Kato, T.; Ito, K.; Amemiya, Y. *Phys. Rev. E* **2000**, *62*, 6865.
(19) Shull, K. R.; Mayes, A. M.; Russell, T. P. *Macromolecules* **1993**, *26*, 3929.
(20) Sferrazza, M.; Xiao, C.; Jones, R. A. L.; Bucknall, D. G.; Webster, J.; Penfold, J. *Phys. Rev. Lett.* **1997**, *78*, 3693.
(21) Senapati, S.; Berkowitz, M. L. *Phys. Rev. Lett.* **2001**, *87*, 176101.
(22) Larson, R. G. *Macromolecules* **1994**, *27*, 4198.

MA062836D